

Kinetic Modeling Application to ^{18}F -fluoroethylcholine Positron Emission Tomography in Patients with Primary and Recurrent Prostate Cancer Using Two-tissue Compartmental Model

Mustafa Takesh^{1,2}

¹Department of Nuclear Medicine, University Hospital Heidelberg, Heidelberg, ²Department of Nuclear Medicine and Radiology, Knappschaft Hospital, 66280 Sulzbach, Germany

Abstract

Although ^{18}F -fluoroethylcholine-positron emission tomography (PET) is the most applied diagnostic method in tumor staging, its role in prostate cancer (PCA) is limited because glucose metabolism tends to be low unless PCA has high Gleason score. Alternatively, choline PET was introduced as a valuable imaging method. Kinetic analysis of PET acquisition has increasingly gained momentum as an investigative tool because it provides a non-invasive approach to obtain kinetic and metabolic data from tissues of interest including transport and metabolism of the administered material. In this regard, we sought to apply it in ^{18}F -fluoroethylcholine (FECH)-PET/computed tomography (CT) in patients with PCA. 64 patients, the mean age 69 (range: 47-87 years) with primary/recurrent PCA were encompassed. They underwent ^{18}F -FECH-PET started with a dynamic acquisition using a 20-frame each 30 s over the prostate region and followed at 1 h post-injection by a static whole body imaging. The kinetic evaluation of the data was performed using the software package PMOD (PMOD Technologies Ltd., Zürich, Switzerland). Significant increase in mean values for K1, K3, FD, standardized uptake value (SUV) and global influx in tumor tissue versus normal tissue ($P < 0.05$). Moderate but significant correlation ($r: 0.28$, $P = 0.023$) between SUV and K1. By contrast, no correlation between SUV and K3 ($r: -0.08$, $P = 0.79$). In patients with recurrent tumors, there is no significant difference in all kinetic parameters and SUV ($P > 0.1$) between the different types of recurrences. The kinetic analysis of dynamic FECH-PET provides a novel method in primary PCA diagnosis and could be of potential value in the delineation of tumor focus.

Keywords: Choline-positron emission tomography, kinetic modeling, prostate cancer

Introduction

It is well-known that increased glycolysis is dominant in most malignancies; thus fludeoxyglucose-positron emission tomography (FDG-PET) is of great value in tumor imaging. However, FDG is not applicable in prostate cancer (PCA) diagnosis because glucose metabolism in

these tumors tends to be low. However, in selected cases such as tumors with a high Gleason score, ^{18}F -FDG-PET can be applied in prostate cancer diagnosis.^[1,2]

Imaging of tumor lipid metabolism has been introduced clinically as an alternative choice, since prostate is characterized by high levels of phospholipid metabolites. Two possible factors contribute to increased choline-uptake. The first is the increased cell proliferation in tumors because choline is a precursor for the biosynthesis of phosphatidylcholine and other phospholipids, the major components of the cell membrane. The second factor is the overproduction of choline kinase in cancer cells compared with normal ones, which was experimentally confirmed in human-derived prostate cancer.^[3-5]

Access this article online

Quick Response Code:



Website:

www.wjnm.org

DOI:

10.4103/1450-1147.136734

Address for correspondence:

Dr. Mustafa Takesh, University Heidelberg, Department of Nuclear Medicine, Im Neuenheimer Feld 400, 69120 Heidelberg, Germany.
E-mail: takesh@stud.uni-heidelberg.de

Owing to the short half-life of ¹¹C, the use of ¹¹C-labeled choline is restricted in centers equipped with cyclotrons on the site, so ¹⁸F labeled choline (fluoroethylcholine [FECH]) is a favorable choice in PCA diagnosis, which show superiority over ¹¹C labeled choline first because of the longer half-life of F-18 (more convenient for a long time storage and long distance transportation). Secondly, the shorter positron range of F-18 provides a slightly higher quality of image and higher spatial resolution.^[6,7]

The diagnostic importance of radionuclide labeled choline had been illustrated in numerous studies including both primary and recurrent tumors, however with multiple shortcomings mainly because of unspecific choline uptake in disorders not related with prostate cancer such as benign prostatic hyperplasia (BPH) and inflammatory changes.^[8] A sensitivity of about 60% and specificity of about 70% have been reported in 2 studies including a total of 67 patients.^[8-10] In clinical practice, the visual evaluation of PET finding in addition to the semi quantitative parameters (standardized uptake value [SUV]) are the main criteria in the delineation of tumor focus. Indeed the uptake observed in static imaging is the sum of multiple succeeding mini processes, which possibly can be assessed by kinetic analysis through a sophisticated program depending on mathematical relations. The resulting model represents the molecular interactions that occur at the cellular level when chemical bonds are reformed into new compounds, enabling thus to understand the tracer distribution in tumor tissue and normal tissue as well. In addition, the applied therapy may be better monitored using this kinetic analysis.^[11]

The choline uptake consists of a set of reaction pathways, rate coefficients for each reaction pathway and reverse rate coefficients. The dynamic PET against static PET may demonstrate these kinetic parameters after choosing the appropriate kinetic model, offering thus the best methodology to understand the uptake mechanism for various clinical and research applications. For example, the knowledge of these elementary reactions can be applied in differentiation between the different types of tissue, which share a choline affinity. In the same context, choline uptake in hyperplastic prostate tissue and other inflammatory disorders including chronic and acute prostatitis had been reported, which in turn decreases the specificity of choline PET for detection and accurate identification of cancer foci within the prostate.^[8] That may emphasize the potential role of kinetic analysis in increasing the specificity of PET finding.

In view of useful conclusions of many studies performed by Strauss *et al.* concerning the kinetic modeling of FDG,^[12] we were encouraged to study the kinetic modeling of choline in a wide variety of prostate cancer manifestations (primary and recurrent tumors), aiming

primarily to highlight the benefit of kinetic analysis of dynamic FECH in demarcating the tumor focus within the prostate gland and to know whether it contributes in increasing the specificity of PET findings or adds further information guiding to the presence of the tumor.

In addition, we assessed the choline kinetic in different recurrence manifestations including lymph node recurrence (LN-R), local recurrence (LR) and bone involvement, aiming to demonstrate a possible relationship of kinetic features with tumor sites. This hypothesis is based on the facts that each tracer has a characteristic in kinetic activity in tumor tissue, which may show a variation in relation to aggression grade and surrounding circumstances including the anatomical locations.

In this topic, it is to be mentioned that the first trail to study kinetic of ¹¹C labeled choline was by Sutinen *et al.* 2003^[13] and less is known regarding the kinetic of FECH in patients with PCA.

Materials and Methods

Patients

Sixty four patients were encompassed in this study. These patients were categorized into two subgroups:

- Those with primary prostate cancer, referred for staging purposes ($n = 19$), the mean age was 66 ± 12 years (range 47-87 years). Mean prostate specific antigen (PSA) value was 18 ± 11 ng/ml (range 6-40). PSA value was not available in 5 patients. Gleason score was available just in ten patients and ranges between 6 and 9.
- Those with biochemical failure after potentially curative therapy and were referred for restaging purposes ($n = 45$), the median age 69 (range 56-84). Gleason score ranges between 5 and 9 and was not available in 10 patients.

Patients in the second group (biochemical failure) had a history of a variety of initial therapy (radical prostatectomy, radiotherapy, high-intensity focused ultrasound, etc.) [Table 1].

The recurrences were distributed as follows: Regional LN-R $n = 16$ (6 pararectal, 4 iliac and 6 inguinal), LR $n = 20$ and bone recurrence $n = 9$ (3 sacrum, 2 acetabulum, 2 ilium and 2 pubis). (Recurrence outside pelvis was excluded from kinetic analysis because the dynamic acquisition was required for this analysis) [Figure 1].

Approximately 50% of all findings were validated through follow-up or by correlation with other available radiological findings. The histological confirmation was available in two findings. The remaining findings were typical.

Table 1: Characteristics of patients with recurrent diseases

Age	PET-Finding	Anatomical position	IT	PSA	GS
73	LN-R	Iliac	RP	0.60	7
83	LN-R	pararectal	RP	5.70	N/A
67	LN-R	Inguinal	RP+RT	1.67	7
64	LN-R	pararectal	RP	27.20	N/A
62	LN-R	pararectal	RP+RT	15.80	N/A
56	LN-R	Inguinal	RP	1.45	7
74	LN-R	pararectal	RP+RT	1.99	N/A
69	LN-R	Inguinal	RP+RT	0.91	5
73	LN-R	pararectal	RP+RT	1.50	7
67	LN-R	Inguinal	RP	4.00	7
67	LN-R	Iliac	RP	1.06	9
73	LN-R	Iliac	NO	20.00	8
74	LN-R	Inguinal	RT	17.00	8
73	LN-R	Iliac	RP	14.50	7
63	LN-R	Inguinal	RP+RT	13.00	7
74	LN-R	pararectal	RP	19.00	7
60	LR	prostate bed	RP+RT	8.50	7
62	LR	prostate bed	RP	4.30	9
69	LR	prostate bed	RT+ AHT	3.00	7
70	LR	prostate bed	RP+RT	0.91	5
66	LR	prostate bed	RP	1.60	7
68	LR	prostate bed	RP	7.40	N/A
74	LR	prostate bed	HIFU	7.50	8
64	LR	prostate bed	RT+HIFU	6.50	7
66	LR	prostate bed	HIFU	2.50	7
76	LR	prostate bed	RT+AHT	1.12	6
84	LR	prostate bed	RT	6.00	7
83	LR	prostate bed	RP	5.70	N/A
67	LR	prostate bed	RP+RT	1.67	7
67	LR	prostate bed	RP+RT	1.50	N/A
68	LR	prostate bed	RT+ AHT	2.40	6
62	LR	prostate bed	RT	4.17	6
72	LR	prostate bed	RT+AHT	29.00	7
73	LR	prostate bed	RT	6.00	7
80	LR	prostate bed	AHT	49.00	N/A
71	LR	prostate bed	RP+RT	4.00	7
59	OSS	Pubis	RT	3.60	8
70	OSS	Sacrum	RP	1.00	7
65	OSS	ilium	RP	4.00	N/A
77	OSS	Acetabulum	RP	6.00	7
68	OSS	Acetabulum	RP	5.00	N/A
71	OSS	Sacrum	RP+RT	12.90	7
61	OSS	sacrum	RP	1.90	8
73	OSS	ilium	RP	21.00	9
62	OSS	Pubis	AHT	14.00	9

LN-R: Lymph node recurrence; LR: Local recurrence, OSS: Bone metastases; IT: Initial therapy; RP: Radical prostatectomy; RT: Radiotherapy; AHT: Antihormonal therapy; HIFU: High-intensity focused ultrasound; GS: Gleason score; N/A: Not available

After transmission scans, a mean dose of 300 MBq (range 250-350 MBq) of [F18] ethylcholine was injected intravenously as a bolus. A dynamic emission acquisition (dPET) in list mode using a 20-frame each 30 s over the prostate region was started simultaneously, followed at 1 h post-injection (p.i) by a static whole body imaging (from head to the proximal femur).

Starting with a dynamic study in both patient groups was of benefit to investigate the prostate bed and the pelvis region before the entrance of radioactive urine in the bladder and ureters, which in turn may complicate the finding assessment [Figure 2].

The acquired data was corrected for dead time, decay and measured photon attenuation. Static images were reconstructed using the ordered subset-expectation maximization algorithm using four iterations with eight subsets and Gauss filtering to an in-plane spatial resolution of 5 mm at full-width half-maximum.

The benefit of accompanied computed tomography (CT) in both dynamic and static study was emphasized not only in attenuation correction but also in anatomical matching of abnormal uptake.

The reconstructed images were converted to SUV images. The mean and maximum SUV 55-60 min post-injection was used for the analysis of uptake in static imaging.

The evaluation of the dPET data was performed with the software package PMOD (PMOD Technologies Ltd., Zürich, Switzerland) using PMOD kinetic modeling tool.

Although a two-tissue compartment model is the standard methodology for the quantification of dynamic ¹⁸F-FDG PET studies, there is no experience in applying this model in the quantification of dynamic ¹⁸F-FECH-PET/CT in patients with prostate cancer. However, in the light of choline track illustrated in [Figure 3], the two-compartment model was supposed to be an appropriate candidate to describe FECH kinetic and for this reason it was selected.

In this model, we assume the physiological tissue is combined of two homogeneous mixed interacting compartments; and the resulting parameter K1 indicates for the choline transport into cells, whereas K3 indicates for trapping of transported choline through choline kinase mediated phosphorylation and subsequent accumulation of phosphocholine, which in turn acts as substrate of further enzymatic steps leading to phosphatidylcholine biosynthesis.

The absence of accurate measurement of the input function, which theoretically requires arterial blood sampling, was a technical problem we faced. However, the input function can be retrieved from the image data with good accuracy. Hence the input curve was created through a volume of interest (VOI) consisting from many region of interest (ROIs) (mostly 5) located over an arterial vessel. In general, the common iliac artery was selected for this purpose.

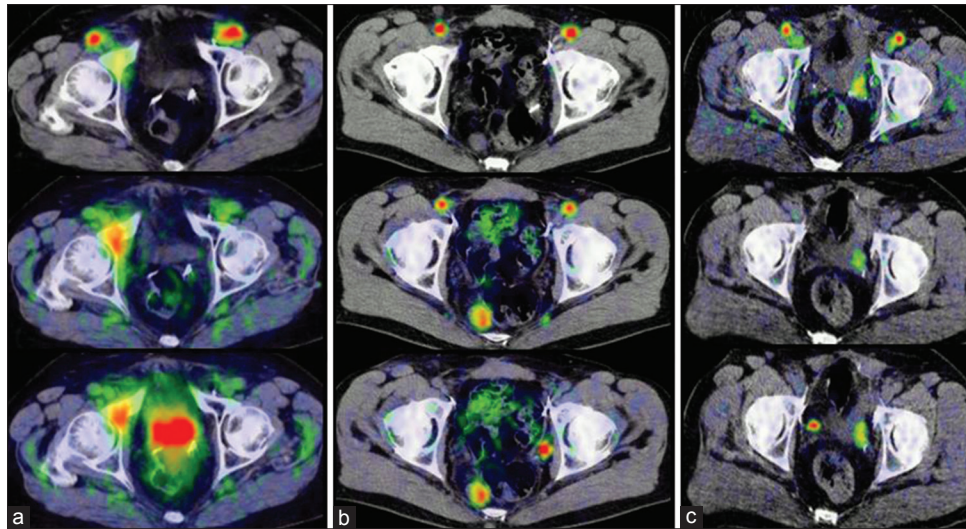


Figure 1: The dynamic acquisition in the three recurrence types selected for kinetic analysis (a). Bone involvement (b). Lymph node involvement (c). Local recurrence. The upper rows represent the first frame of dynamic phase (radioactivity in arteries); the lower rows represent the end of dynamic phase (note the radioactivity in bladder and ureter); the middle rows represent the mid-dynamic phase

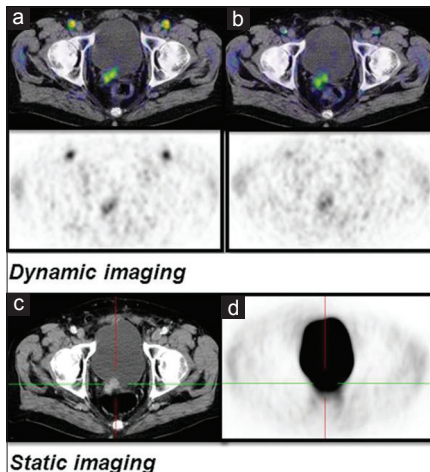


Figure 2: A 77-year-old prostate cancer-patient was referred due to prostate-specific antigen relapse. (a) Axial planes of ¹⁸F-fluoroethylcholine-positron emission tomography/computed tomography (¹⁸F-FECH-PET/CT) fused image and pure PET respectively in the early dynamic phase show a suspected choline uptake in the dorsal bladder wall suggestive for a local recurrence (LR) (notice the radioactivity in the femoral arteries). (b) Axial planes of ¹⁸F-FECH-PET/CT fused image and pure PET respectively in the middle dynamic phase still show the suspected LR (activity decline in the femoral arteries). (c) Contrast-enhanced pelvis CT shows the upper described suspected LR with contrast enhancement. (d) Static image of ¹⁸F-FECH-PET (axial plane) failed to demonstrated the described LR, since it was superimposed by the radioactivity in the bladder, showing thus the importance of dynamic phase in detecting the LR

For tissue time activity curves (TAC), a VOI consisting of many ROIs was drawn at the last frame over target tissue as follows:

In patients with primary PCA: A VOI was placed over the tumor focus within the prostate gland; another VOI was placed over the adjacent normal tissue. For accurate drawing over the target area, it was sometimes necessary

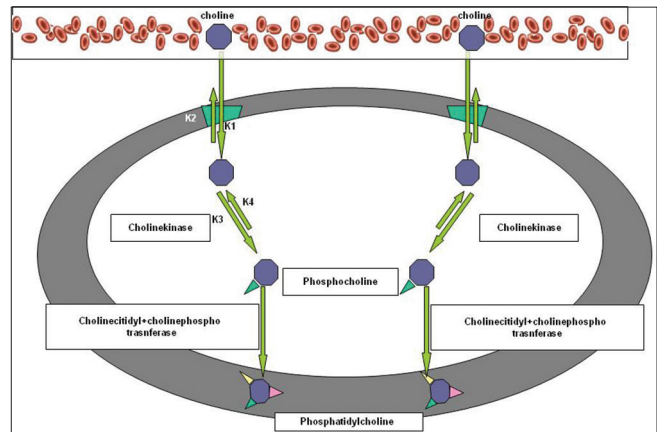


Figure 3: Compartment model in the light of choline metabolism

to make fusion imaging with CT, taking advantage from its anatomical guiding [Figure 4].

Likewise, in patients with recurrences (LN-R, LR and bone involvement) a VOI was placed over the recurrence focus for tumor tissue TAC, in addition to VOIs over iliac arteries for input curve. For reference tissue in both patients groups another VOI was placed in the gluteal muscle.

Procedures done to achieve the highest anatomical correlation

After data import, the reconstructed dynamic acquisition was revised and analyzed in several displays (transaxial, sagittal and coronal) as well as in several time points (frame by frame), tumor focus was defined as a hot spot mostly at the last frame (10 min p.i.). VOIs in a dynamic phase were placed over the hot spot in accordance with static findings (reviewing of static imaging was essential before dynamic analysis) [Figure 4].

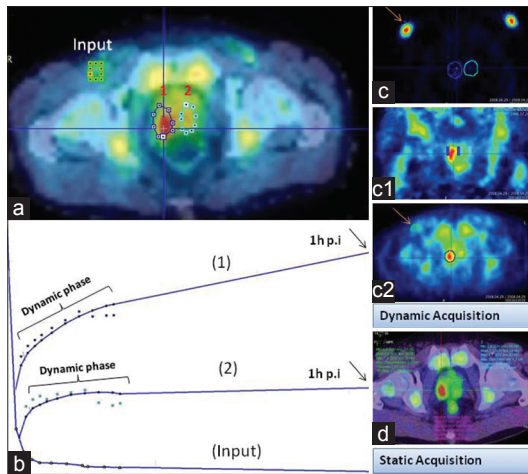


Figure 4: (a) ^{18}F -fluoroethylcholine-positron emission tomography/computed tomography fused image (axial plane) show the volume of interest drawing over tumor focus and adjuvant normal tissue within prostate gland with corresponding time activity curves and input curve (b). (c) Acquisition point at the beginning of dynamic phase (radioactivity in the arteries) (c1, c2) coronal and axial planes at the end of the dynamic phase show a tumor focus in the right prostatic lobe. (d) Fused image (axial plane) in the static imaging (1 h post-injection) shows the tumor focus in the right prostatic lobe corresponding thereby with the dynamic phase

After VOIs configuration, we added the SUV value retrieved from the static images 1 h p.i. in order to interpolate the kinetic activity within the whole hour as follows:

- For the late value of tumor tissue TAC (primary or recurrence), we entered SUVmean obtained from static imaging by placing VOI over the tumor focus.
- The late value of input curve (suggested to be equal to the blood pool value) was obtained manually by placing a VOI over the heart or big central vessels (on average 1 SUV).
- For the late value of reference tissue TAC (muscle), we entered SUVmean obtained from static imaging by placing VOI over the gluteal muscle (on average 0.5).

All these SUVs were entered in the kinetic analysis using (Add additional time) option in PMOD program. The main purpose from adding these late values was to demonstrate the metabolite process occurring during 1 h and not only in the first 10 min. (as discussed later 10 min dynamic study is not sufficient to encompass the whole metabolic process).

After entering the late values, kinetic model configuration and kinetic model fitting we obtained the following parameters with unit 1/min for each rate constants: K1, K2 assumed to represent the transport into and out of the cells respectively; and K3, K4 which are supposed to represent phosphorylation and dephosphorylation of labeled choline respectively. In addition, we calculated the global influx of ^{18}F -FECH from the compartment data using the formula: $\text{Influx} = (K1 \times K3)/(K2 + K3)$.

After entering the cells, choline can be either metabolized by choline kinase or can be washed out of the cells by back transport until equilibrium is reached. Due to the shortness of the dynamic measurement, this equilibrium cannot be achieved; therefore K2 is not absolutely reliable. Chi-square was the indicator, we considered to validate the kinetic analysis (equal or less than 10 was designated as validation value).

In addition to the compartment analysis, a non-compartment model was used to calculate the fractal dimension (FD). The aim of the model was to calculate the FD of the time-activity data. The FD is a parameter to assess the heterogeneity of the tracer kinetics and was calculated for each VOI using the time-activity data. The values of the FD vary from 0 to 2 showing the more deterministic or chaotic distribution of the tracer activity via time in a local volume defined by a VOI. No input function is needed for the FD model.^[12]

Parametric images were further retrieved from dPET. Images of the slope and the intercept of the time-activity data have been calculated using the PMOD software using pixel-wise modeling tool. Parametric images of the slope reflect the trapping of ^{18}F -FECH thus K3, whereas the parametric images of the intercept reflects the distribution volume of ^{18}F -FECH thus K1. The parametric images were evaluated visually.

Statistical analysis

Mean, median and standard deviation were the main statistical methods. The comparison between data had been performed using static graphic program software package on a personal computer (Intel® Pentium® Processor T4200 (2.0 GHz, 800 MHz FSB) NVIDIA GeForce G 105M up to 1791 MB TurboCache) running with Windows Vista Home Premium. Descriptive statistics and box plots were used for the analysis of the data. $P < 0.05$ was considered to be statistically significant.

Results

The tumor foci showed mostly besides the enhanced ^{18}F -FECH uptake an increased phosphorylation rate and volume of distribution in the parametric images [Figure 5].

Kinetic analysis in primary prostate tumor: (Tumor tissue vs. adjuvant tumor tissue)

The descriptive statistics of all evaluated parameters including the SUVs, transport constant K1 and rate constants (K2 – K4), as well as the FD of the ^{18}F -FECH kinetics in malignant and benign tissues are presented in Tables 2 and 3.

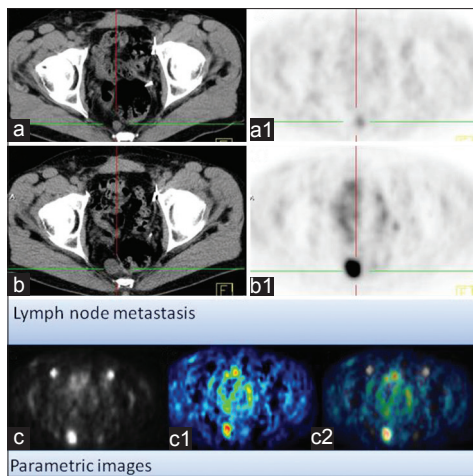


Figure 5: A 64-year-old prostate cancer-patient was referred to our department with prostate-specific antigen (PSA) relapse after radical prostatectomy (PSA serum level 11.5 ng/ml) (a, a1). Baseline ^{18}F -fluoroethylcholine-positron emission tomography (^{18}F -FECH-PET) and corresponding computed tomography (CT) (axial plane) demonstrates decent increased uptake in an enlarged lymph node (LN) pararectal (maximum standardized uptake value [SUVmax] 2.3). (b, b1). Follow-up ^{18}F -FECH-PET and corresponding CT (axial plane), 6 months later exhibits an increasing in both volume and uptake (SUVmax 9.9), confirming thus a LN metastasis as cause of PSA relapse. Parametric images intercept image (c), slope image (c1), intercept/slope fusion (c2) showing an increased phosphorylation rate and volume of distribution in the upper demonstrated LN metastasis

The data show increased mean values for all parameters in tumor tissue. The *t*-test revealed a significant difference of the mean values for K1, K3, FD, SUV and global influx ($P < 0.05$) [Figure 6].

Although the median value for the both K1 and K3 appear to be higher for malignant tissue compared with normal tissue, the overlap of the extreme values for both group was noticeable, likewise in the FD.

Kinetic parameters in recurrent PCA

The mean value and standard deviation of kinetic and static parameters including the SUVs, rate constants (K1 – K4), Influx as well as the FD of the ^{18}F -FECH kinetics in various recurrence types are presented in [Table 4]. The kinetic results counting K1, K3, influx in addition to FD and SUV value in 16 patients with lymph node (LN) metastases (4 iliac, 6 pararectal and 6 inguinal) have the following median and range values 0.74 (range 0.07-0.99), 0.11 (range 0.01-0.95), 0.16 (range 0.02-0.52), 1.09 (range 0.7-1.21) and 5.5 (range 5-9), respectively (Chi-squared values of more than 10 were excluded from statistical analysis).

In patients with LR (N. 20), The kinetic parameters K1, K3, influx besides FD and SUV have the following median and range values 0.54 (range 0.24-0.99), 0.13 (range 0.02-0.89), 0.13 (range 0.05-0.45), 1.12 (range 1.03-1.26) and 5.20 (range 2.7-16), respectively.

Table 2: Descriptive statistics for all malignant tissues

Variable	No. of lesions	Minimum	Maximum	Median	Mean \pm SD
^{18}F -FECH (SUV)	19	1.96	7.7	3.9	4.17 \pm 1.4
K1 (1/min)	19	0.26	0.99	0.67	0.66 \pm 0.24
K2 (1/min)	19	0.06	0.99	0.3	0.31 \pm 0.21
K3 (1/min)	19	0.0001	0.99	0.38	0.36 \pm 0.33
K4 (1/min)	19	0.0001	0.95	0.21	0.34 \pm 0.32
Influx	19	0.001	0.72	0.23	0.29 \pm 0.23
FD	19	0.96	1.3	1.11	1.09 \pm 0.1

FECH: Fluoroethylcholine; SUV: Standardized uptake value; FD: Fractal dimension; SD: Standard deviation

Table 3: Descriptive statistics for all normal tissues

Variable	Minimum	Maximum	Median	Mean \pm SD
^{18}F -FECH (SUV)	1.54	3.5	2.7	2.6 \pm 0.5
K1 (1/min)	0.2	0.8	0.33	0.39 \pm 0.19
K2 (1/min)	0.07	0.6	0.19	0.24 \pm 0.15
K3 (1/min)	0.0001	0.82	0.01	0.14 \pm 0.25
K4 (1/min)	0.0001	0.99	0.06	0.26 \pm 0.34
Influx	0.00	0.44	0.02	0.07 \pm 0.11
FD	0.84	1.16	0.97	0.97 \pm 0.09

FECH: Fluoroethylcholine; SUV: Standardized uptake value; FD: Fractal dimension; SD: Standard deviation

By contrast, in patients with bone involvement ($n = 9$), the kinetic parameters K1, K3, influx besides FD and SUV have the following median and range values 0.77 (range 0.14-0.99), 0.12 (range 0.001-0.99), 0.12 (range 0.01-0.68), 1.14 (range 0.83-1.29) and 4.7 (range 2.3-9), respectively. They were distributed as follows: 3 sacrum, 2 ilium, 2 pubis, 1 acetabulum and 1 in ischium.

Statically, in comparison between kinetic parameters in all clinical manifestations bone metastasis (OSS), local recurrence (LR), lymph node recurrence (LN-R), there is no significant difference in all kinetic parameters (K1, K3, influx and FD) as well as in SUV ($P > 0.1$).

SUV versus kinetic parameters in all tumor manifestation including (primary tumor, LR, LN-R and OSS)

The ^{18}F -FECH-uptake 1 h p.i. is supposed to be determined by choline transport into a tumor cell and the subsequent choline phosphorylation. That suggests presence of association between SUV (static acquisition) and kinetic parameters (dynamic acquisition). In relation SUV with K1, we found a moderate but significant correlation ($r: 0.28, P = 0.023$). By contrast, there was no correlation between SUV and K3 ($r: -0.08, P = 0.79$) [Figure 7].

Accordingly, SUV is more related with the extent of choline transport represented by K1 than with choline metabolism represented by K3.

Table 4: Descriptive statistics for patients with recurrent tumors

R-type	No.	¹⁸ F-FECH (SUV)	K1 (1/min)	K2 (1/min)	K3 (1/min)	K4 (1/min)	FD	Influx
LN-R	16	5.2±2	0.65±0.2	0.36±0.25	0.26±0.3	0.27±0.3	1.06±0.11	0.17±0.15
LR	20	6.3±3.4	0.64±0.27	0.43±0.25	0.21±0.23	0.10±0.14	1.11±0.06	0.17±0.1
BM	9	5.7±2.8	0.69±0.3	0.36±0.18	0.31±0.35	0.09±0.12	1.09±0.15	0.24±0.27

LN-R: Lymph node recurrence; LR: Local recurrence; BM: Bone metastasis; FECH: Fluoroethylcholine; SUV: Standardized uptake value; FD: Fractal dimension

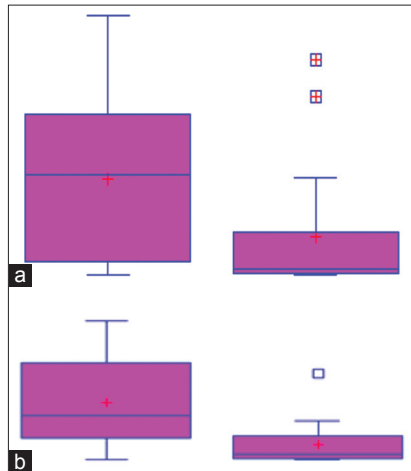


Figure 6: Comparison between tumor and normal tissue in the values of (a) K3 and (b) Influx respectively, the statistic is summarized as box plot

Gleason score in relation with kinetic parameters and SUV

In all tumor manifestations, there were no correlation between GS and kinetic parameters.

In details: GS versus K3 ($r: 0.25, P = 0.13$), GS versus K1 ($r: 0.25, P = 0.14$) and GS versus FD ($r: 0.06, P = 0.74$).

As well as, there was a poor correlation between GS and SUV ($r: 0.13, P = 0.55$).

Discussion

High specific detection of prostate cancer within the prostate gland using imaging modality is of increasing value, considering the growing concern to perform a guided focal therapy.

Of course, the biopsy is still the main procedure to confirm the tumor. However, owing to the likelihood of false negative, a fraction of patients are referred to surgery in spite of negative biopsy. That emphasizes the importance of a high specific diagnostic method.

The normal prostate gland is characterized by “aerobic glycolysis” since the Krebs cycle and consequently oxidative phosphorylation is inhibited. In prostate cancer, citrate metabolism is shifted to citrate oxidation in the Krebs cycle. So, prostate cancer tissue demonstrates decreased levels of citrate and increased levels of choline.^[8,14]

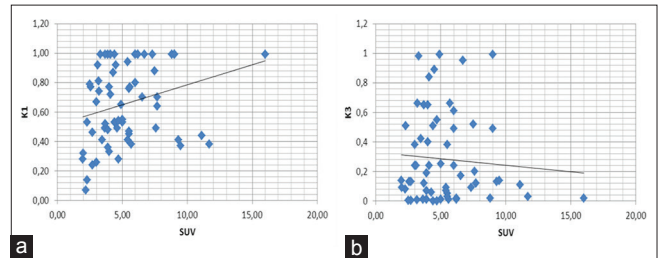


Figure 7: The relationship of SUV with K1 and K3 respectively, presented in scatter plot. (a) SUVmean vs. K1 ($r: 0.28 P = 0.023$). (b) SUV mean vs. K3 ($r: -0.08 P = 0.79$)

These metabolic characteristics of prostate cancer play a role in prostate cancer imaging, such as in magnetic resonance imaging-spectroscopy, here a strong magnetic field is used to get metabolic information.

Elastography application from ultrasound may be useful in the correct detecting of PCA within the prostate gland. A study by Salomon *et al.* described good results of elastography in this topic.^[15]

In nuclear medicine, ¹⁸F-FDG PET/CT is the most commonly used tumor imaging technique. However, it is well-established that prostate tumor utilizes the fatty acids and choline while glucose utilization and thus FDG-uptake is minimal. The role of ¹⁸F-FDG PET is limited, unless in PCA with high Gleason score. Effert *et al.* even found that ¹⁸F-FDG PET could not differentiate prostate cancer from benign prostate hyperplasia.^[16,17]

As mentioned earlier, the prominent metabolic process in PCA that may be utilized for imaging purposes is the overexpression of fatty acid synthesis and overexpression of choline kinase. Choline kinase phosphorylates free choline to phosphocholine, which is the initial step of choline metabolism and then in many steps eventually forms phosphatidylcholine, the major constituent of the cell membrane.^[8]

PET with radiolabeled choline either labeled with ¹⁸F or ¹¹C has been found to be most useful in prostate cancer. ¹⁸F-FECH-PET/CT demonstrated superiority over ¹¹C labeled choline first due to the longer half-life of F18 (more convenient for a long time storage and long distance transportation), second due to the shorter positron range of F18, providing a slightly higher quality of image with higher spatial resolution.^[6,7]

Choline uptake from hyperplastic prostate tissue and other inflammatory disorders including chronic and acute prostatitis had been reported. That decreases specificity of choline PET for detection and accurate identification of cancer foci within the prostate.^[8]

Depending on histopathologic findings, a sensitivity of about 60% and specificity of about 70% have been reported in 2 studies including a total of 67 patients.^[8-10]

The first event of choline accumulation in tumor cells is transport across the membrane by various transporters. Since choline is a polar molecule, uptake by passive diffusion is low. There are 3 known choline transport systems in human cells classified functionally as low affinity, high affinity and intermediate affinity.^[8,18]

The difference in choline uptake in tumor tissue versus normal tissue can be best explained by the varying activation of previously mentioned transport systems, second by increased micro vessel density (MVD). Since K1 represents tracer transport into the cells, it is not surprising that a significant difference in K1 exists in tumor tissue compared with normal tissues. As mentioned earlier, prostate tumor is characterized with overexpression of choline kinase. That may explain the significant difference in K3 in tumor tissue compared with normal tissue since K3 is a kinetic parameter supposed to represent choline metabolism.

Choline uptake usually plateaus within 10-20 min after injection.^[8,19] Experimental studies have indicated that a large fraction of intracellular choline still presents as non-metabolized choline.^[8,20]

This fact suggests that choline transport and not the phosphorylation is the key factor for choline uptake, which reaches the peak 10-20 min after injection, validating thus our results in discovering that SUV is more correlated with K1 than with K3 (results).

Concerning the contribution of choline kinase in the choline uptake Henriksen *et al.*^[21] found in their *in vitro* experiments on human prostate cancer cells that the signal obtained by imaging early after injection mainly reflects the transport. Thus, K3, as a valid quantification of choline kinase activity, needs imaging at later time points. That had also been confirmed using a choline derivative (¹⁸F-dehydroxycholine), which cannot be phosphorylated by choline kinase. It was shown that this derivate uptake was similar to choline at early time points (10 min after injection). At later time points, however, uptake of choline was significantly higher than ¹⁸F-dehydroxycholine, indicating that phosphorylation by choline kinase increases intracellular trapping of choline and choline kinase activity can affect the *in vivo* PET-signal.

For this reason, we tried to assess the kinetic activity of choline during 1 h instead of 10 min (dynamic period), in order to demonstrate the role of choline kinase, which occurs in delay and thus to make the parameters more reliable.

Although it is difficult to distinguish between the contribution of choline transport and choline metabolism in choline uptake, it is obvious that, choline transport is dominant in the first minutes, whereas choline kinase gets involved in internalization mostly in the later time period.

A study by Iorio *et al.* found a significant increase in choline kinase to 12-24 fold higher values in comparison to non-tumor cells and tried via nuclear magnetic resonance to distinguish between transport and phosphorylation. They demonstrated that at short incubation time, (5 min) radiolabeled internalization was largely dependent on the choline transport while at longer incubation times (>20 min) choline phosphorylation became the dominant step in cellular enrichment.^[22]

The same observation was demonstrated with our data when taking into account only the first 10 min of the dynamic study. As a result, we found the predominance of K1 in tumor tissue. By contrast, taking into account the late value 1 h p.i. both, K1 and K3, were significantly increased in tumor tissue. Therefore, the kinetic analysis of choline taking also into account the static value of 1 h p.i. provides a more reliable model about choline kinetics which may add some validation to the static PET findings. However, it may be of more value to compare the kinetic activity in PCA with that of other findings suggested to cause false positive findings in ¹⁸F-FECH-PET/CT (e.g. inflammation, BPH).

FD is another non-compartmental approach that can be added to the previous mentioned parameters in characterizing the tumor tissue. As demonstrated in our results the FD in tumor tissue differs significantly from normal tissue ($P < 0.001$). Moreover, this approach has the main advantage that no input function is needed and it appears to be less related with operator-experience.

In addition to choline transport, K1 is supposed to be further determined by angiogenesis and MVD. It is known that tumor angiogenesis is the main trigger factor in prostate cancer whether in the primary tumor or in recurrent tumor and has been shown in several studies to be associated with tumor aggression.

Angiogenesis can be assessed by counting the microvessels within a tumor focus, which is based on immunohistochemical assays applied to histologic sections which contain a sufficient amount of tumor

tissue.^[23] This microvessel count was considered as another pathological approach except for GS to predict the tumor aggression. This technique might also help to identify patients with a high likelihood for developing metastases and to select them to undergo more aggressive adjuvant therapy. Wakui *et al.* found that blood capillary density ratio was significantly higher in prostate carcinomas that developed bone marrow metastases.^[24]

Gleason score was not confirmed to be correlated with microvessel density, so tumor angiogenesis and tumor-cell proliferation are regulated by different mechanisms.^[25]

In multivariate analysis Weidner *et al.* showed that microvessel count added significantly more information than GS in predicting the risk of metastasis.^[23]

Theoretically, the angiogenesis may be estimated to some extent using the kinetic analysis, taking into account that K1 reflects also the nuclide availability through angiogenesis. Under this suggestion, we might predict the tumor aggression and select the patients with a high likelihood to develop metastasis to undergo aggressive therapy. However, in our patients there was no long follow-up to prove this hypothesis. This correlation between K1 and the incidence of metastases requires further long-term studies.

In the related context, the parametric images are methods for feature extraction based on dedicated algorithms and they enable to visualize the single perfusion contribution of choline uptake. Intercept images are supposed to reflect the perfusion-dependent part of ¹⁸F-FECH-uptake (K1), whereas the second type (slope) is assumed to reflect the extent of phosphorylation rate (K3). These images can be easily calculated and do not need any input data.

Using intercept images, we can estimate the amount of microvessels in the primary tumor, thus predicting the aggression of tumor. In recurrence as well, it can be estimated to which extent the metastases are perfused, which may play a role in selecting further therapy.

By looking at the kinetic parameters in different types of recurrences, including LR, LN-R and bone involvement, we found that the kinetic activity of choline did not turn out to be related with tumor site in evidence of similarity in resulting parameters. Given to the lack of difference of FD between all recurrence manifestations, we suggest that the radiopharmakon distributes similarly in different tumors sites.

In an attempt to show the relation between GS and K3, which is supposed to represent choline kinase, we

found a poor correlation between GS and K3 ($r = 0.25$; $P = 0.13$). In the same topic, Bhakoo *et al.* reported similar results and found that choline kinase activity and phosphocholine levels were generally not well correlated with proliferation rates.^[26,27]

Likewise, Gleason score does not correlate with SUV ($r = 0.13$; $P = 0.55$) matching with the *in vivo* study performed by Breeuwsma *et al.* who found that choline uptake does not correlate with cell proliferation in human prostate cancer.^[4]

Ultimately, after developing new radio immunotherapy for prostate cancer the kinetic analysis of FECH could be of major advantage in early prediction of therapy response mimicking thereby the confirmed role of kinetic analysis of dFDG. That could be a main topic of future research.

Conclusion

The kinetic analysis of dynamic ¹⁸F-FECH provides a novel method in prostate cancer diagnosis and could be of potential value in the delineation of tumor foci. This may in turn grant further characterization of tumor focus other than SUV value retrieved from static image.

The kinetic of choline doesn't vary with tumor location, taking into account the homogeneity in the kinetic parameters found in comparison between different recurrence-types counting LR, LN involvement and bone involvement.

References

1. Oyama N, Akino H, Suzuki Y, Kanamaru H, Sadato N, Yonekura Y, *et al.* The increased accumulation of [¹⁸F] fluorodeoxyglucose in untreated prostate cancer. *Jpn J Clin Oncol* 1999;29:623-9.
2. Kanamaru H, Oyama N, Akino H, Okada K. Evaluation of prostate cancer using FDG-PET. *Hinyokika Kyo* 2000;46:851-3.
3. Beheshti M, Langsteger W, Fogelman I. Prostate cancer: Role of SPECT and PET in imaging bone metastases. *Semin Nucl Med* 2009;39:396-407.
4. Breeuwsma AJ, Pruijm J, Jongen MM, Suurmeijer AJ, Vaalburg W, Nijman RJ, *et al.* *In vivo* uptake of [¹¹C] choline does not correlate with cell proliferation in human prostate cancer. *Eur J Nucl Med Mol Imaging* 2005;32:668-73.
5. Zheng QH, Gardner TA, Raikwar S, Kao C, Stone KL, Martinez TD, *et al.* [¹¹C] Choline as a PET biomarker for assessment of prostate cancer tumor models. *Bioorg Med Chem* 2004;12:2887-93.
6. Hara T, Kosaka N, Kishi H. Development of (18) F-fluoroethylcholine for cancer imaging with PET: Synthesis, biochemistry, and prostate cancer imaging. *J Nucl Med* 2002;43:187-99.
7. Lavery HJ, Brajtford JS, Levinson AW, Nabizada-Pace F, Pollard ME, Samadi DB. Unnecessary imaging for the staging of low-risk prostate cancer is common. *Urology* 2011;77:274-8.
8. Plathow C, Weber WA. Tumor cell metabolism imaging. *J Nucl Med* 2008;49 Suppl 2:43S-6.

9. Testa C, Schiavina R, Lodi R, Salizzoni E, Corti B, Farsad M, *et al.* Prostate cancer: Sextant localization with MR imaging, MR spectroscopy, and ¹¹C-choline PET/CT. *Radiology* 2007;244:797-806.
10. Farsad M, Schiavina R, Castellucci P, Nanni C, Corti B, Martorana G, *et al.* Detection and localization of prostate cancer: Correlation of (¹¹) C-choline PET/CT with histopathologic step-section analysis. *J Nucl Med* 2005;46:1642-9.
11. Dimitrakopoulou-Strauss A, Strauss LG, Egerer G, Vasamillette J, Schmitt T, Haberkorn U, *et al.* Prediction of chemotherapy outcome in patients with metastatic soft tissue sarcomas based on dynamic FDG PET (dPET) and a multiparameter analysis. *Eur J Nucl Med Mol Imaging* 2010;37:1481-9.
12. Strauss LG, Klippel S, Pan L, Schönleben K, Haberkorn U, Dimitrakopoulou-Strauss A. Assessment of quantitative FDG PET data in primary colorectal tumours: Which parameters are important with respect to tumour detection? *Eur J Nucl Med Mol Imaging* 2007;34:868-77.
13. Sutinen E, Nurmi M, Roivainen A, Varpula M, Tolvanen T, Lehtikoinen P, *et al.* Kinetics of [(¹¹) C] choline uptake in prostate cancer: A PET study. *Eur J Nucl Med Mol Imaging* 2003;31:317-24.
14. Kurhanewicz J, Vigneron D, Carroll P, Coakley F. Multiparametric magnetic resonance imaging in prostate cancer: Present and future. *Curr Opin Urol* 2008;18:71-7.
15. Salomon G, Köllerman J, Thederan I, Chun FK, Budäus L, Schlomm T, *et al.* Evaluation of prostate cancer detection with ultrasound real-time elastography: A comparison with step section pathological analysis after radical prostatectomy. *Eur Urol* 2008;54:1354-62.
16. Dimitrakopoulou-Strauss A, Strauss LG. PET imaging of prostate cancer with ¹¹C-acetate. *J Nucl Med* 2003;44:556-8.
17. Effert PJ, Bares R, Handt S, Wolff JM, Büll U, Jakse G. Metabolic imaging of untreated prostate cancer by positron emission tomography with ¹⁸fluorine-labeled deoxyglucose. *J Urol* 1996;155:994-8.
18. Michel V, Yuan Z, Ramsbair S, Bakovic M. Choline transport for phospholipid synthesis. *Exp Biol Med (Maywood)* 2006;231:490-504.
19. Hara T, Kosaka N, Kishi H. PET imaging of prostate cancer using carbon-11-choline. *J Nucl Med* 1998;39:990-5.
20. Bansal A, Shuyan W, Hara T, Harris RA, Degrado TR. Biodisposition and metabolism of [(¹⁸) F] fluorocholine in 9L glioma cells and 9L glioma-bearing fisher rats. *Eur J Nucl Med Mol Imaging* 2008;35:1192-203.
21. Henriksen G, Herz M, Hauser A, Schwaiger M, Wester HJ. Synthesis and preclinical evaluation of the choline transport tracer deshydroxy-[¹⁸F] fluorocholine ([¹⁸F] dOC). *Nucl Med Biol* 2004;31:851-8.
22. Iorio E, Mezzanzanica D, Alberti P, Spadaro F, Ramoni C, D'Ascenzo S, *et al.* Alterations of choline phospholipid metabolism in ovarian tumor progression. *Cancer Res* 2005;65:9369-76.
23. Weidner N, Carroll PR, Flax J, Blumenfeld W, Folkman J. Tumor angiogenesis correlates with metastasis in invasive prostate carcinoma. *Am J Pathol* 1993;143:401-9.
24. Wakui S, Furusato M, Itoh T, Sasaki H, Akiyama A, Kinoshita I, *et al.* Tumour angiogenesis in prostatic carcinoma with and without bone marrow metastasis: A morphometric study. *J Pathol* 1992;168:257-62.
25. Vartanian RK, Weidner N. Endothelial cell proliferation in prostatic carcinoma and prostatic hyperplasia: Correlation with Gleason's score, microvessel density, and epithelial cell proliferation. *Lab Invest* 1995;73:844-50.
26. Aboagye EO, Bhujwala ZM. Malignant transformation alters membrane choline phospholipid metabolism of human mammary epithelial cells. *Cancer Res* 1999;59:80-4.
27. Bhakoo KK, Williams SR, Florian CL, Land H, Noble MD. Immortalization and transformation are associated with specific alterations in choline metabolism. *Cancer Res* 1996;56:4630-5.

How to cite this article: Takesh M. Kinetic Modeling Application to ¹⁸F-fluoroethylcholine Positron Emission Tomography in Patients with Primary and Recurrent Prostate Cancer Using Two-tissue Compartmental Model. *World J Nucl Med* 2013;12:101-10.

Source of Support: Nil, **Conflict of Interest:** None declared.